# Intrinsic conductance variability in Ge-rich GST ePCM bitcells: a characterization study

A. Motta[1], M. Baldo[1], E. Petroni[1], G. Samanni[1], E. Palumbo[1], E. Gomiero[1], R. Annunziata[1] and A. Redaelli[1]
[1]TR&D STMicroelectronics, Agrate Brianza, Italy

***Abstract*— This study presents the first comprehensive analysis of intrinsic variability in the conductance of amorphous and crystalline states in Ge-rich GST ePCM bitcells. Electrical data from both states were statistically evaluated. Detailed physical TEM analyses were performed, and Monte Carlo modeling of conductance distributions was developed. The results are discussed, identifying the main source of variability. Amorphous conductance dispersion is attributed to the electronic transport influenced by the density of localized states within the bandgap. Crystalline conductance dispersion arises from a modulation of Sb content in the structure of the active dome.**

***Keywords—ePCM, Ge-rich GST, intrinsic variability, modeling***

## I. INTRODUCTION

Across the different technologies for embedded Non-Volatile Memories (eNVM), embedded Phase Change Memories (ePCM) based on Ge-rich GeSbTe (GST) alloy were demonstrated to fulfill all the requirements for consumer, industrial and automotive applications [1,2,3,4]. A distinctive feature of Ge-rich GST alloy is the forming operation, which activates and homogenizes the alloy of the bitcells to achieve optimal programmability [5]. Following this, the programming operation defines a highly conductive crystalline SET state and a low-conductive amorphous RESET state. The conductance (*G*) distributions of the SET and RESET states across an array of bitcells exhibit intrinsic variability. This work starts by investigating the evolution of intrinsic variability in relation to the forming operation. Then, a comprehensive electrical statistical analysis is performed alongside physical characterization. Bitcells from different quantiles of the conductance cumulative distribution in both crystalline and amorphous states are selected for physical imaging analysis to examine their morphological structure and chemical composition. Finally, relations are derived to express the SET and RESET conductance as functions of the physical bitcell parameters. Using these relations, SET and RESET state distributions are then simulated via Monte Carlo (MC) method and compared with measured data, providing valuable insights into the sources of intrinsic conductance variability.

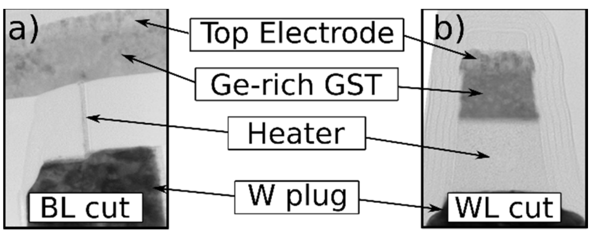


Fig. 1. STEM cross section of the ePCM cell. The active material (Ge-rich GST) and the heater are highlighted. In a) is shown the cross section along the Bit-Line (BL) direction, in b) along the Word-Line (WL) direction.

## II. IMPACT OF FORMING OPERATION

A dedicated array was developed with an integrated multiplexer that enables addressing each single bitcell. All signals for programming, reading, addressing and power supplies were delivered by a Keysight B1500 parameter analyzer. The cell architecture is a Ge-rich GST Wall ePCM and two different technology nodes were used: 90 nm, represented in Fig.1 [2], and 28 nm [4]. The influence of the forming operation on the intrinsic variability in the conductance was evaluated by performing a full characterization of each individual bitcell in the 90 nm array. In the pristine state, before any electrical forming and programming pulse application, bitcells exhibit a low and broad conductance distribution [7]. Staircase up-and-down voltage pulses [6] were used to collect *I-V* and *G-I* curves. The array was divided into sectors of 200 bitcells, each subjected to increasing levels of forming current. As shown in Fig.2, the dispersion in the *G-I* curves decreases as the forming current increases. The normalized standard deviation of conductance calculated at each programming current point along the *G-I* curve converges after a specific forming current level. This suggests that the ability of the forming process to reduce the cell-to-cell variability reaches a saturation point. The residual variability can be seen in the curves reported in Fig.3 and will be analyzed in detail in the next sections.

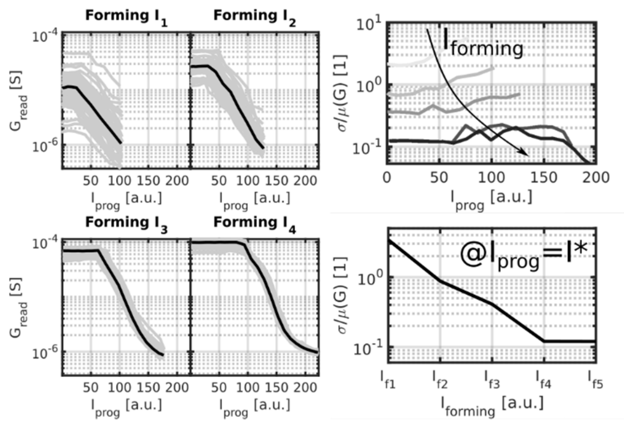


Fig. 2. Left half. Evolution of the *G-I* characteristics at different forming current levels. From $I_1$ to $I_4$ the current of the forming pulse increaes. Light shades of gray represent the *G-I* curves of each of the 200 bitcells, while the black curve represents the median of the group. Cell-to-cell variability decreases significantly with increasing forming current level. Right half. Top: conductance dispersion normalized by the mean for each current programming level at different forming levels. Increasing forming levels are represented by darker shades. Bottom: graph shows the conductance dispersion normalized by the mean converging at high forming current levels with fixed programming.

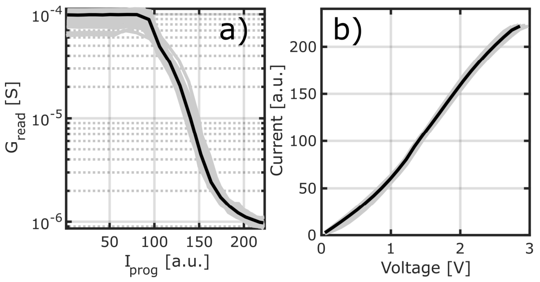


Fig. 3. In a) conductance-current (*G-I*) and in b) current-voltage (*I-V*) characteristics at the chosen forming current level for this study. Cell-to-cell variability is reduced by applying the chosen forming pulse, which minimizes the normalized standard deviation as shown in Fig.2.

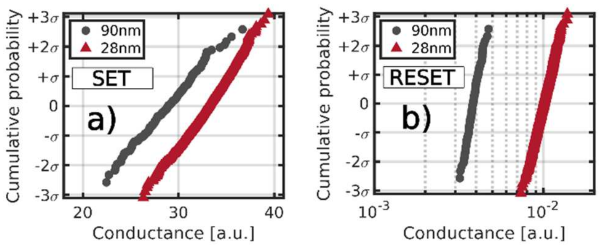


Fig. 4. In a) SET and in b) RESET cunductance distributions of in two different ePCM technology nodes.

## III. Statistical and Physical Analysis

More than 200 bitcells were programmed into SET and RESET states, and their respective conductance cumulative distributions are reported in Fig.4. The SET state has data with good linear fit, indicating that its distribution follows a normal probability distribution function. In contrast, the RESET state has cumulative distribution that appears linear when plotted on a logarithmic scale, suggesting that it follows a lognormal probability distribution function. This result was confirmed on both the technology nodes. Topological differences between bitcells, like un-uniform program and read voltage distributions or geometrical differences, were ruled out due to absence of spatial correlations in the state values as shown in Fig.5. The SET and RESET state are not correlated both within the pristine state and with each other.

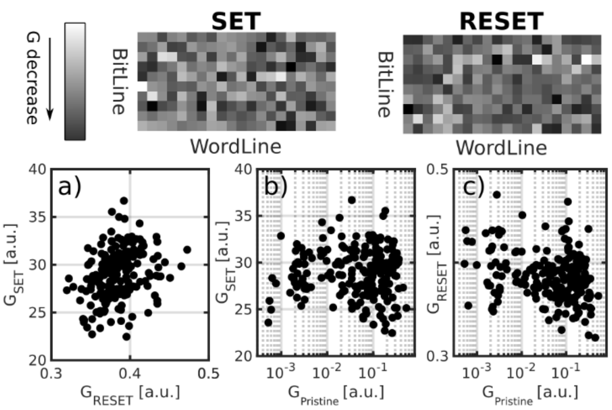


Fig. 5. On top spatial distribution on the considered die of SET and RESET conductance. On the bottom correlation plots between different important cell states. a) shows how there is no correlation between SET and RESET state conductance. b) and c) show how there is no influence of the initial pristine state on both SET and RESET state and therefore that the forming pulse correctly homogenizes and uniforms the material.

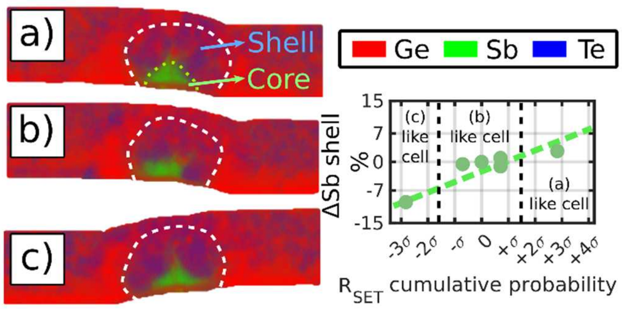


Fig. 6. EELS images of three different cells at different positions in the SET distribution: a) high conductivity extreme b) median c) low conductivity extreme. There are no notable differences in morphology. Composition analysis shows that the Sb content in the shell increases with higher SET conductance values.

To investigate the physical difference between bitcells corresponding to different distribution quantiles, specifically those in the high and low extremes as well as the median, Scanning Transmission Electron Microscopy (STEM) techniques were employed, including Electron Energy Loss Spectroscopy (EELS) and Dark Field (DF-STEM) imaging. The SET state exhibits a crystalline phase, compositionally divided into a core and a shell [8]. In particular, antimony (Sb) is the element that promotes conduction. As shown in Fig.6, the Sb-rich core remains unmodulated, while the Sb concentration within the shell increases at higher SET conductance levels. This compositional variation clearly explains the observed intrinsic variability. For the RESET state, Fig.7 shows that the size and chemical composition, especially the Sb content, of the amorphous dome do not exhibit significant variation across different statistical levels of RESET conductance. To further validate the non-contributory role of dome size, a dedicated electrical measurement was performed. In this experiment, groups of bitcells were programmed at different current levels with RESET programming currents equal to their forming currents, ensuring the same chemical composition in the amorphous dome [8]. The results, reported in Fig.8, indicate that the median conductance value does not significantly change despite dome size modulation, which was indirectly monitored by measuring the threshold switching voltage [9]. Therefore, the source of RESET variability requires further investigation into electronic transport.

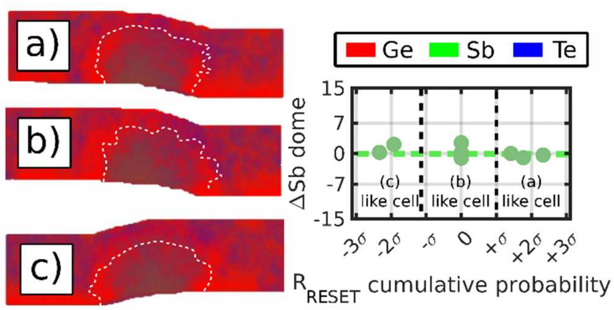


Fig. 7. On the left, EELS images show the extent of the amorphous region (highlighted with a white dotted line drawn from the associated STEM images) and the overall composition. Red represents Ge concentration while blue Te and green Sb. Physical images of three RESET states at different positions in the conductance cumulative distribution: a) high conductivity extreme b) median c) low extreme. On the right, Sb content modulation relative to the Sb content median shows no compositional differences among the three amorphous domes.

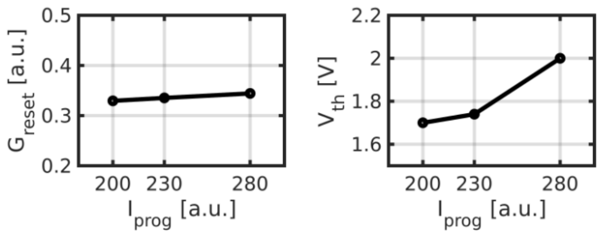


Fig. 8. Trends of RESET conductance and threshold voltage (Vth) as functions of programming current (equal to forming current).

## IV. Modeling

Analytical relations for RESET and SET state conductance as functions of main physical and cell parameters were derived based on the cell geometry illustrated in Fig.9. The main component for the RESET conductance is the low-conductive amorphous active dome. The latter has a symmetry along the GST line width which simplifies the problem to two dimensions. The conductance $G_{RESET}$ is then calculated as the reciprocal of the resistance along the path from the top part of the heater to the dome radius $u_d$, integrating the series resistance contribution of infinitesimal semicircles. The resulting relation, shown in Fig.9 (a), expresses the RESET state conductance as function of the radius $u_d$ and the conductivity $\sigma_{RESET}$ of the amorphous dome. The non-linear dependence on the dome radius was compared with the TCAD numerical solution of the Laplace equation $\nabla^2 V = 0$ with Dirichlet boundary conditions applied to the top electrode and the heater, as shown in Fig.9 (c). Good agreement is observed between the equipotential voltage lines calculated from the derived relation and those obtained from the Laplace equation solution. As an example, a voltage profile along the GST line thickness is presented in Fig.9 (d). The Poole-Frenkel electronic transport mechanism was then considered to model the dependence of conductivity $\sigma_{RESET}$ on temperature and read voltage [9], as shown in Fig.10.

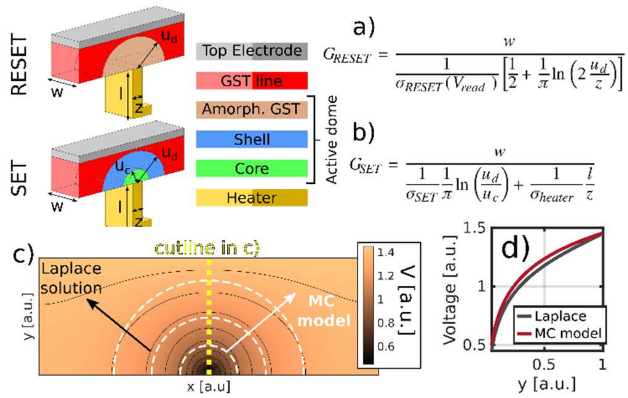


Fig. 9. Equations used in the Monte-Carlo model for RESET (a) and SET (b) state conductance with $u_d \geq z$ and $u_c \leq u_d$. On the top left, a schematic of the bitcell is represented with annotations indicating all the different dimensions considered. c) TCAD solution of the Laplace equation for a bitcell geometry with thin heater and large top electrode. White lines are voltage iso-lines from the MC model, while black lines are from the Laplace solution. d) Difference along the symmetry axis shown in c) between the two solutions. The error between the two methods is negligible, justifying the approximation used.

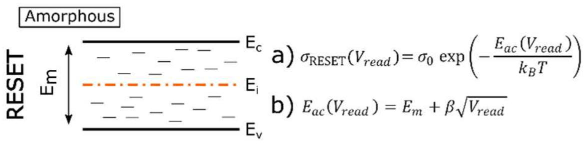


Fig. 10. On the left, representation of the band diagram for amorphous Ge-rich GST conduction in accordance with [9]. On the right, the formulas used in the Monte Carlo model to represent the conductivity of the RESET state.

Carrier transport occurs via thermally activated hopping between positively charged localized states that generate potential barriers modulated by the read voltage. The activation energy $E_{ac}$ comprises the mobility gap $E_m$ and the beta parameter $\beta$, which are primarily related to the material composition and density of localized states, respectively, as in Fig.10 (b). Similarly, for the SET state, the conductance relation $G_{SET}$ was calculated by including contributions from the shell region and the heater in series as reported in Fig 9 (b). It was assumed that the Sb-rich core, with its high conductivity, and the pristine region between the active dome and the top electrode make only minor contributions [8]. The RESET and SET conductance distributions were then simulated using the Monte Carlo (MC) method. All parameters from the previous equations (dome radius, mobility gap, beta parameter, SET conductivity and cell geometry) were assumed to be normally distributed and mutually independent. Their values were randomly sampled from their respective distributions and then inserted into the previously calculated relations to generate the simulated conductance distributions. Each parameter was then analyzed in terms of its contribution to the intrinsic variability of RESET and SET conductance.

## V. Discussion

The RESET and SET conductance distributions were analyzed using the discussed MC model. The cell geometry factors related to heater element (line width $w$, thickness $z$, height $l$ and conductivity $\sigma_{heater}$ as shown in Fig.9) were previously calibrated using the linear part of the *I-V* curve, whose slope is correlated to the heater resistance. For the RESET state, the amorphous dome radius $u_d$ was constrained to be smaller than the thickness of the GST line and its standard deviation was tuned to prevent correlation between conductance $G_{RESET}$ and dome radius, ensuring consistency with the previous TEM result. A lognormal conductivity $\sigma_{RESET}$ distribution is considered because of its exponential dependence on $E_m$ and $\beta$. The MC distribution matched well with the measured data, as shown in Fig.11, considering a 6% relative dispersion in conductivity, which is the highest among the dispersions of the other physical parameters, around 1-3%.

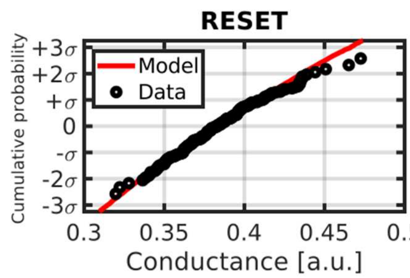


Fig. 11. RESET conductance distribution from measured data and from the Monte Carlo model result.

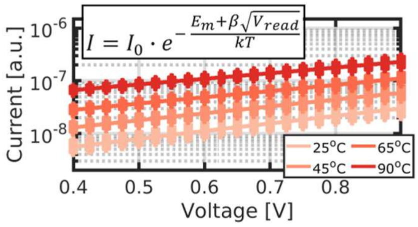


Fig. 12. *I-V* curves for a group of cells at different temperatures. In the box the formula used to model the current voltage dependance.

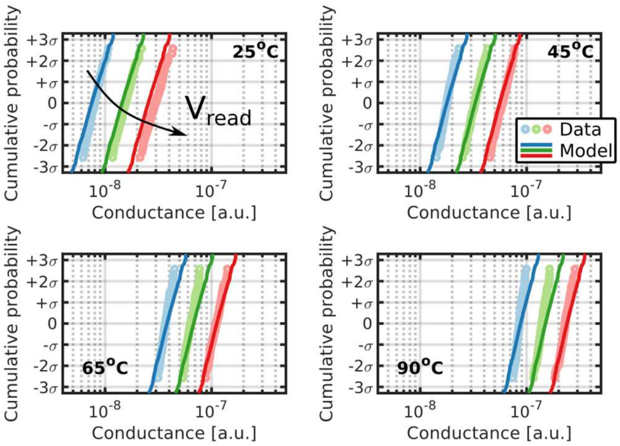


Fig. 13. RESET conductance distributions at three levels of applied read voltage (in different colors) at multiple temperatures. Dots represent the measured data, while lines indicate the Monte Carlo model results. A good match is observed for all voltages and temperatures considered.

This provides evidence that the main source of RESET state variability lies in the amorphous conductivity $\sigma_{RESET}$, specifically in electronic transport. Finally, to evaluate separately the $E_m$ and $\beta$ contributions on the conductivity, subthreshold RESET *I-V* curves were measured over a range of read voltages and temperatures, as shown in Fig.12. The RESET current equation is expressed as a function of $E_m$ and $\beta$ (Fig.12). The RESET conductance distributions at various read voltages and temperatures were simulated with the same MC method previously described. Results show a good match with the measured distributions (Fig.13), considering $\beta$ relative dispersion 10 times higher than the $E_m$ relative dispersion. This clearly indicates that the density of localized states is the primary source of intrinsic variability in RESET conductance. The correlation between conductance with its drifted value, as shown in Fig.14, confirms this evidence. In fact, the conductance drift over time is a process caused by the localized states [9].

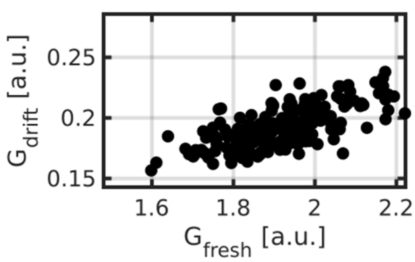


Fig. 14. Correlation between fresh (just after program operation) and drifted RESET conductance value.

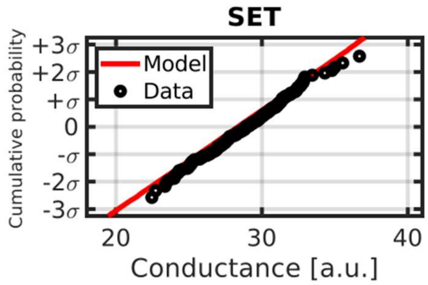


Fig. 15. SET conductance distribution from measured data and from the Monte Carlo model result.

The same MC procedure was applied to analyze the SET conductance distribution. The relation, shown in Fig.9 (b), has the same constraint on the active dome radius as previously discussed for the RESET state. The simulated conductance distribution was successfully compared with the measured data, as shown in Fig.15, assuming a 10% relative dispersion of the shell region conductivity, which is again the highest value among the other parameter dispersions, around 1-3%. This evidence is consistent with the Sb content modulation in the shell observed through physical TEM analysis.

## VI. Conclusions

Intrinsic variability in the RESET and SET conductance in Ge-rich ePCM bitcells was studied through electrical and physical characterizations. The analysis began with the impact of the forming operation, which is a characteristic of Ge-rich GST alloys. It revealed that intrinsic variability is modulated by this operation; specifically, it decreases and reaches a saturation point as the forming current amplitude increases. Statistical review shows that RESET and SET conductance values of bitcells, whose distributions follow lognormal and normal distributions respectively, are not correlated either within the pristine state or with each other. EELS and DF-STEM techniques, combined with Monte Carlo modeling, were applied to investigate the main sources of intrinsic variability in the RESET and SET conductance. The results demonstrate that intrinsic dispersion is primarily governed by the density of localized states in the bandgap for RESET conductance and by antimony content modulation in the shell structure of the active dome for SET conductance.

## References

[1] A. Redaelli et al., IEDM, 2024, pp. 1-4, doi: 10.1109/IEDM50854.2024.10873404.

[2] G. Croce, IMW, 2022, pp. 1-4, doi: 10.1109/IMW52921.2022.9779244.

[3] F. Disegni et al., Symposium on VLSI Circuits, 2021, pp. 1-2, doi: 10.23919/VLSICircuits52068.2021.9492465.

[4] F. Arnaud et al., IEDM, 2020, pp. 24.2.1-24.2.4, doi: 10.1109/IEDM13553.2020.9371934.

[5] E. Palumbo et al., Solid-State Electronics, vol 133, pp. 38-44, 2017, https://doi.org/10.1016/j.sse.2017.03.016

[6] E. Gomiero et al., IEEE Journal of the Electron Devices Society, vol. 7, pp. 517-521, 2019, doi: 10.1109/JEDS.2019.2913467

[7] M. Baldo et al., 2020, pp. 13.3.1-13.3.4, doi: 10.1109/IEDM13553.2020.9372089.

[8] Ran, S. et al., Sci Rep 15, 11357 (2025). https://doi.org/10.1038/s41598-025-95227-z

[9] D. Ielmini et al. J. Appl. Phys. 2007. https://doi.org/10.1063/1.2773688